LA-UR-21-22095
Approved for public release; distribution is unlimited.

Title: Magnetic velocity gauges: Effects of misalignment

Author(s): Menikoff, Ralph

Intended for: Note for colleagues and coworkers

Issued: 2021-03-02

Magnetic velocity gauges: Effects of misalignment

Ralph Menikoff

March 1, 2021

1 Introduction

Embedded velocity gauges are standardly used at LANL on gas gun experiments of a shock-to-detonation transition; see fig. 1. The experiments are intended to be one-dimensional with a planar shock driven by the projectile from a gas gun propagating along the axis of the HE cylinder. The accuracy of the gauges depends on the alignment of the directions of shock propagation, magnetic field and the active gauge element.

A source of inaccuracies is from tilt or misalignment angle at impact between the projectile surface and the HE surface; typically a few milliradians. This leads to the shock propagating at a slight angle to the axis of the HE cylinder and can affect the shock rise time of the velocity gauges, the time offset between the tracker gauges for the trajectory of the lead shock, and the gauge positions in the direction of propagation.

It is important to note that tilt is characterized by 2 parameters; the magnitude of the angle relative to the HE axis and the direction in the plane transverse to the HE axis. Here we derive the uncertainties from tilt to leading order in the tilt angle.

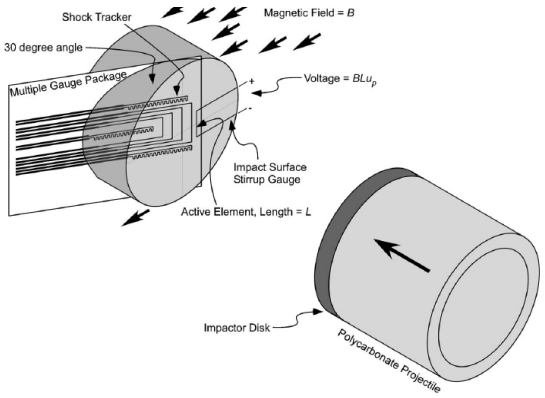

Figure 1: Sketch of embedded gauge package in a gas gun experiment from [Gustavsen et al., 2006, fig 1].

2 Tilt angle

As noted by Gustavsen et al. [2012, §III.B], the impact tilt angle and the shock tilt angle are related by Snell's law. For small angles, this reduces to

$$\theta_s = (u_s/u_{proj}) \cdot \theta_{impact} \ , \tag{1}$$

where u_{proj} and u_s are the projectile and initial shock speed in the HE, respectively, and the angles are in radians; see fig. 2.

Equation (1) is a geometrical relation and represents the property for a steady wave pattern that the velocities of the node (intersection of waves) calculated from the incoming and outgoing waves are the same. Moreover, for small angles, to leading order in θ the shock speed is determined by the 1-D shock impedance match between the projectile and the HE.

Since the velocity ratio u_s/u_{proj} is greater than one, the tilt angle for the HE shock is greater than the tilt angle for the projectile at impact. Moreover, for a given u_s, the velocity ratio is larger for a projectile with a stiffer EOS, such as sapphire. In addition, the velocity ratio is larger for a lower initial HE shock pressure.

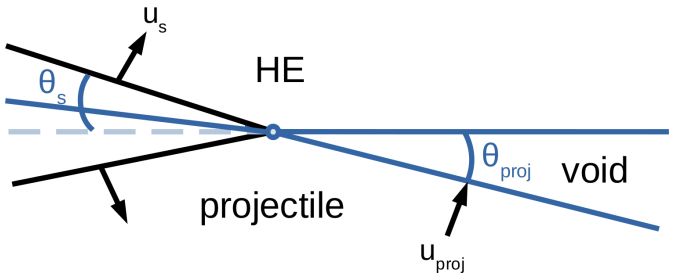

Figure 2: Wave pattern for projectile impact with tilt. Blue lines are contact waves (material interfaces) and black lines are shock waves. The node is the blue circle where the waves intersect.

3 Gauge geometry

With perfect alignment the directions of the magnetic field ($\hat{B}$), the active element of the gauges ($\hat{a}$), and shock propagation ($\hat{u}$) are mutually orthogonal. We use the co-ordinate system in which these directions are along the x-, y- and z- axes, respectively. In addition, the direction of the gauge package (conductors to the active gauge element) is typically at an angle of 30° with respect to the plane of the shock front or 60° relative to the z-axis.

The gauge package angle is analogous to the configuration for the older wedge experiments used to determine Pop plot points for a shock-to detonation transition. The large phase velocity for the shock arrival along the gauge package outruns the shock reflection off the gauge package. Consequently, the tracker gauges determine the 1-D lead shock trajectory. In addition, the velocity gauges cover a range of positions along the shock direction.

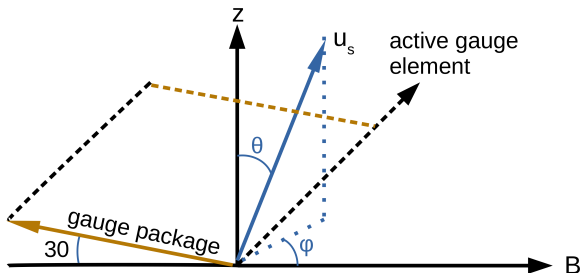

Figure 3: Coordinate axes for magnetic gauge package.

The principal directions can be expressed as follows

$$\hat{B} = \big(1, 0, 0\big) \ , \tag{2a}$$
$$\hat{a} = \big(0, 1, 0\big) \ , \tag{2b}$$
$$\hat{g} = \big(\cos(30^\circ), 0, \sin(30^\circ)\big) \ . \tag{2c}$$

Tilt will alter the direction of shock propagation. It can be expressed as

$$\hat{u} = \big(\sin(\phi)\sin(\theta), \cos(\phi)\sin(\theta), \cos(\theta)\big) \ , \tag{2d}$$

where the polar angle θ is the magnitude of the tilt angle, and the azimuthal angle ϕ is the direction projected in the transverse plane; see fig. 3. With angles in radians, $0 \le \phi < 2\pi$, and to leading order for small tilt $\sin(\theta) \approx \theta$ and $\cos(\theta) \approx 1$.

Shock rise time: Let ℓ be the length of the active gauge element. Then the time for the lead shock to cross the gauge element is

$$\Delta t = (\ell/u_s)\, \hat{u} \cdot \hat{a} \approx (\ell/u_s)\cos(\phi)\, \theta \ , \tag{3}$$

where u_s is the shock speed at the gauge position. Thus, the gauge rise time gives a lower bound on the tilt angle; $\Delta t\, u_s/\ell \le \theta$. Moreover, the rise time vanishes if $\phi = \pi/2$, *i.e.*, the active element of the gauge is in the plane of the shock front. Similarly, tilt will give a time offsets among the left, right and center tracker gauges.

When the lead shock is strong enough to trigger fast reaction, the rise time leads to inaccuracies in determining the particle velocity behind the shock front.

Magnetic flux: The measured output voltage of the gauge is proportional to the time derivative of the magnetic flux (Faraday's law)

$$\mathsf{d}(flux)/\mathsf{d}t = (u\, B\, \ell)\, \hat{B} \times \hat{a} \cdot \hat{u} = u\, B\, \ell\, \cos(\theta) \approx u\, B\, \ell \ , \tag{4}$$

where u is the particle velocity of the active gauge element and B is the magnitude of the magnetic field. Assuming the active element of the gauge moves with the particle velocity of the HE, to leading order, tilt does not affect the measured particle velocity.

However, Bdzil [2018] has raised the issue for an oblique magnetic gauge that there may be a shear layer along the active element of the gauge which would cause the gauge particle velocity to differ from the HE particle velocity. This is seen in 2-D hydro simulations of a shock passing over the gauge; see for example Menikoff [2021]. The velocity difference due to slip would be a systematic error with the velocity measurement rather than a random error.

Gauge position scaling: The initial gauge positions are projected onto the direction of shock propagation. Without tilt

$$z = z_0 + \ell\, \hat{g} \cdot \hat{z} = z_0 + \tfrac{1}{2}\ell \ , \tag{5}$$

where z_0 is the position of the start of the gauge package from the front surface of the HE, and ℓ is the distance along the gauge package transverse to the active elements.

With tilt the gauge position is

$$z = z_0 \cos(\theta) + \ell\, \hat{g} \cdot \hat{u} \approx z_0 + \ell \left[\sin(\phi)\cos(30^\circ)\,\theta + \sin(30^\circ)\right] = z_0 + \tfrac{1}{2}\ell + \left[\tfrac{\sqrt{3}}{2}\,\sin(\phi)\,\theta\right] \ell \ . \tag{6}$$

We note that the tilt correction for the gauge position vanishes when the shock rise time from Eq. (3) is maximum and vice versa. Furthermore, the scaling of the tracker gauge positions from tilt gives rise to a systematic error in the shock speed rather than a random error.

After the transition to detonation, the gauge position scaling from tilt would cause the detonation speed from the slope of the tracker gauges to differ from the planar CJ detonation speed by a factor of $1 + \frac{\sqrt{3}}{2}\,\sin(\phi)\,\theta$. In principle, the inaccuracy from position scaling can be corrected for if the tilt angles θ and ϕ are measured.

Alternatively, if the run distance is long enough for a steady detonation wave to be reached then the ratio of the final slope of the tracker trajectory to the CJ detonation speed from another experiment can be used to determine the scaling factor. Simulations of shock-to-detonation transition experiments show that for sensitive explosives with a CJ reaction-zone width of less than 0.1 mm, the steady state detonation speed is reached within a couple of mm of the transition to detonation.

References

J. B. Bdzil. Fluid Mechanics of an Obliquely Mounted MIV Gauge. Technical report, Los Alamos National Lab., March 2018. LA-UR-18-22397.

R. L. Gustavsen, S. A. Sheffield, and R. R. Alcon. Measurements of shock initiation in the tri-amino-tri-nitro-benzene based explosive PBX 9502: Wave forms from embedded gauges and comparison of four different material lots. *J. Appl. Phys.*, 99:114907, 2006. URL http://dx.doi.org/10.1063/1.2195191.

R. L. Gustavsen, R. J. Gehr, S. M. Bucholtz, R. R. Alcon, and B. D. Bartram. Shock initiation of triaminotrinitrobenzene base explosive PBX 9502 cooled to -55 C. *J. Appl. Phys.*, 112, 2012. URL http://dx.doi.org/10.1063/1.4757599.

R. Menikoff. xRage simulations of magnetic velocity gauges used in gas gun shock initiation experiments. Technical Report LA-UR-21-21769, Los Alamos National Lab., 2021.